# Modeling the formation of double rolls from heterogeneously patterned gels

Oz Oshri, Santidan Biswas, and Anna C. Balazs

# Modeling the formation of double rolls from heterogeneously patterned gels

Oz Oshri,[1, *] Santidan Biswas,[1] and Anna C. Balazs[1]

[1]*Chemical Engineering Department, University of Pittsburgh, Pittsburgh, Pennsylvania 15261*
(Dated: February 6, 2019)

Both stimuli-responsive gels and growing biological tissue can undergo pronounced morphological transitions from 2D layers into 3D geometries. We derive an analytical model that allows us to quantitatively predict the features of 2D-to-3D shape changes in polymer gels that encompasses different degrees of swelling within the sample. We analyze a particular configuration that emerges from a flat, rectangular gel that is divided into two strips ("bi-strip"), where each strip is swollen to a different extent in solution. The final configuration yields double rolls that displays a narrow transition layer between two cylinders of constant radii. To characterize the rolls' shapes, we modify the theory of thin, incompatible elastic sheets to account for the Flory-Huggins interaction between the gel and the solvent. This modification allows us to derive analytical expressions for the radii, the amplitudes and the length of the transition layer within a given roll. Our predictions agree quantitatively with available experimental data. In addition, we carry-out numerical simulations that account for the complete non-linear behavior of the gel, and show good agreement between the analytical predictions and the numerical results. Our solution sheds light on a stress focusing pattern that forms at the border between two dissimilar, soft materials. Moreover, models that provide quantitative predictions on the final morphology in such heterogeneously swelling hydrogels are useful for understanding growth patterns in biology, as well as accurately tailoring the structure of gels for various technological applications.

## I.    Introduction

Morphogenesis is the process by which biological organisms develop their shape. This process typically encompasses the growth of new tissue [1–4], which enables such events as: the reshaping of epithelial sheets [5, 6], the development of plants and leafs [7–10], and the emergence of surface morphologies on living organs [11–13]. The growth of biological tissue involves the addition of mass to an evolving structure; if the structure is formed from an elastic material, the growth commonly drives a two-dimensional (2D) shape to transition into a three-dimensional (3D) configuration [1, 14]. In particular, the addition of mass to the 2D architecture introduces in-plane strains that can only be relaxed by the material's reconfiguration into a 3D morphology. To gain insight into physicochemical factors that can affect the transition of 2D layers into 3D structures and the subsequent elastic relaxation within the material, researchers have focused on morphological transitions that can be induced in hydrogels. Notably, polymeric hydrogels [15] can mimic the mechanical behavior of biological tissues [16] and have been used extensively as tissue replacements [17, 18]. Moreover, while biological growth processes are in general time-dependent, such as cell division or accretion of surfaces [2], in many cases the time-scales for the subsequent elastic relaxations are much faster than these dynamical evolutions. Therefore, at least to leading order, non-stationary effects can often be neglected [2, 3]. Hence, the understanding of 2D-to-3D shape changes in hydrogels of finite, fixed size can yield significant insight into shape changes within biological tissue.

Herein, we derive an analytical model that allows us to quantitatively predict the features of 2D-to-3D shape changes in polymer gels that encompass different degrees of swelling within the sample. Such gels can be realized, for example, by introducing variations in the cross-link density within the network or polymerizing the chains to be relatively longer in one area of the sample than another. Models that provide quantitative predictions on the final morphology in such heterogeneously swelling hydrogels would be useful not only for understanding growth patterns in biology, but also for accurately tailoring the structure of gels to meet the requirements of various technological applications.

Pattern formation in thin sheets where a given sample displays different degrees of deformation or buckling yields a particularly rich set of morphologies. Kim et al. [19] investigated the latter scenario experimentally by manipulating thin gels into 3D configurations. In these experiments, the cross-link densities in the gels were tuned by a differential exposure to UV light. The intensity of light that illuminated each portion of the gel determined its ability to swell within an aqueous medium. Using this method, the researchers could drive the thin sheets to form cones, spherical caps and wavy patterns, and more complex morphologies such as self-folded cubes and axisymmetric rolls.

* ozo2@pitt.edu

We focus on the experimental setup of Ref. [20] where a rectangular flat sample of a thin gel was divided into two strips that were manipulated to undergo differential swelling, i.e., one strip was programmed to swell more than the other. This "bi-strip" system was then activated in a thermal liquid bath until its final 3D configuration was achieved. The resulting shapes consisted of two cylindrical rolls, each with a different constant radius, that are connected by a sharp transition layer. This transition layer encompasses large deformations of the gel over very short distances and thereby ensures a smooth transition between the two rolls. These rolls occurred repeatedly for different sized samples, which were of different lengths and thickness. Scaling arguments, which are based on the competition between stretching and bending energies, were then utilized to explain the various dependencies of the rolls' radii on the initial size of the gel. Considering the simplicity of this approach, the authors were able to predict the experimental observations to within good agreement.

Researchers have also considered a closely related system [21, 22], which involved an array of thin hydrogel strips with alternating chemical compositions that was designed to mimic biological fibrous tissues. When these patterned gels came into contact with a liquid bath, the different strips underwent distinct degrees of swelling, similar to the behavior in Ref. [20]. Depending on the size and orientation of the strips, these hydrogels formed helical structures with measurable handedness and pitch, and rolls with periodic undulations in the radius (similar to rolls seen in Ref. [20]). Given the ubiquitous appearance of these basic shapes in biology and their reproducibility in experimental studies, there is a need for more quantitative studies on structure formation in differentially-swelling gels. To address this need, we focus on the fundamental building block in these structures, i.e., the bi-strip.

In particular, we develop an analytical model that accounts for the different elastic properties of the two strips. Since the swelling of a gel changes the elastic response of the network, our model takes into consideration the changes in the thicknesses and the Young's moduli of each strip. Consequently, by direct comparison with the experimental data, we show that the elastic theory for thin sheets, supplemented by corrections to the elastic properties of the gel, captures the quantitative behavior of the system, including the numerical prefactors. Utilizing this result we can analyze a stress focusing structure that forms on the border between two dissimilar materials, i.e., materials with different elastic properties. Although stress concentration in thin elastic sheets has been explored extensively [23], the latter scenario was given less attention. Indeed, the localization that we observe herein does not coincide with other known groups of stress focusing patterns, but rather shares properties with two different groups.

The theory is further validated by comparing the findings from the analytical model with the results from computer simulations utilizing the gel lattice spring model (gLSM), which is a modified finite-element method [24–26]. These numerical simulations solve the complete elastodynamics formulation for the mechanical behavior of the gels and were successful in describing the dynamics of lower critical solution temperature (LCST) gels such as Poly(N-isopropylacrylamide) (PNIPAM). Recently, this technique was modified to account for gels that contain loops, which unfold to release "stored length" in the sample [27]. These loops are polymer chains that can form new bonds between two distant points in the network. The creation or annihilation of these bonds effectively mimics a decrease or an increase in the rest length of line elements in the gel. Consequently, the agreement between the simulations, the theory and the experiments shows the predictive capability of our model and sheds light on the various assumptions that lead from the mechanics of gels to the elasticity of thin sheets.

The paper is organized as follows. In Sec. II, we formulate the problem and derive the constitutive relations between the strains and the displacement fields. In Sec. III, we utilize this formulation to obtain an approximate analytical solution for a buckled shape in the framework of the Föppl-von Kármán (FvK) theory. These theoretical predictions are then tested against the numerical optimization of the energy and the gLSM simulations. In Sec. IV, we compare the analytical solution to the experimental data of Ref. [20] and explain the matching between the theoretical and the experimental parameters. Lastly, in Sec. V, we compare the properties of our localizing pattern with other known stress focusing structures, and classify it accordingly. Finally, we summarize our main results and suggest extensions for future studies.

## II. Mathematical formulation of the problem

Our aim is to derive the set of equations that will allow us to determine the 3D configuration of thin gel that encompasses different degrees of swelling. The relevant physical parameters of the system are the dimensions of the gel, the degree of swelling within each region, and the stretching and bending moduli of the sample. To capture the final structure of the swollen, buckled gel, we must derive an expression for the elastic energy, the stress-strain relations and the appropriate constitutive equations. Below, we first provide a qualitative description of our approach and then detail our derivation of the analytical expressions.

To formulate a model for 2D-to-3D shape changes in polymer gels, it is useful to recall that the mechanical behavior of hydrogels is influenced by three distinct factors [24, 28–31]. One is the materials elasticity, which accounts for the non-linear (neo-Hookean) response of the polymeric network [25]. Second is the enthalpic interaction between the

polymers and the surrounding solvent, which is characterized by the Flory-Huggins interaction parameter [30], and third is the non-linearity in the fluid dynamics that guarantees the conservation of mass of both the polymers and the solvent. This nonlinear formulation for the mechanics of gels is relatively simplified when the following two assumptions are considered: (i) the 3D gel samples are thin, i.e., the thickness is negligibly small compared to the two other dimensions, and (ii) only time-independent deformations are considered. Since thin objects can undergo large deformations while the in-plane strains remain relatively small, the finite elasticity model, with neo-Hookean stress-strain relations, can be reduced to a linear elastic model with Hookean relations. In addition, when only static deformations are considered, the Flory-Huggins model and the equations for conservation of mass are only utilized to determine the constant moduli of the linear elastic theory [25]. This simplification of the theory into linear elasticity, supplemented by the standard Kirchhoff-Love hypothesis for dimensional reduction from 3D to 2D [32, 33] allows one to formulate the mechanics of thin cross-linked gels solely using the theory of thin elastic sheets. Indeed, this similarity motivated experimental and theoretical studies of pattern formation on thin gels [21, 34–39].

Although the in-plane deformations of a thin sheet are assumed to be small, the relations between the strains and the displacement fields are not linear. This nonlinearity is associated with the geometry of the final configuration, rather than the nonlinearity in the neo-Hookean model, which accounts for finite strains. Therefore, on top of the linear elastic formalism of thin sheets, another assumption of "smallness" is frequently applied. Namely, in the Föppl-von Kármán (FvK) theory (or small slope approximation), the constitutive relations describing the thin sheets are approximated by the leading order of the gradients in the deformation. The Föppl-von Kármán (FvK) theory has been employed in many recent studies on pattern selection in thin sheets and gels [32, 40–43].

In the following discussion, the term "incompatible sheets" refers to thin films that contain internal stresses even in the absence of external forces [35, 44–47]. Mathematically, incompatible sheets are modeled by a reference metric, $\bar{g}$, that is attached to the mid-plane of the elastic sheet and determines the rest-lengths of line elements on the sheet. Utilizing Gauss's theorem [48, 49], one finds that a flat sheet is stress free only if $K_{\bar{g}} = 0$, where $K_{\bar{g}}$ is the Gaussian curvature of the reference configuration. In other words, when $K_{\bar{g}} \neq 0$ and the sheet is flat not all line elements can retain their rest values simultaneously.

The final 3D configuration of an incompatible sheet is determined by minimization of its total elastic energy. To leading order, this energy scales as $E \propto t(a - \bar{g})^2 + O(t^3)$, where $a$ is the metric of the deformed state, $t$ is the thickness, and the first and second terms correspond respectively to the stretching of in-plane line elements and out-of-plane bending. Therefore, in the limit of a small thickness, the energy is minimized when $a \to \bar{g}$, or equivalently, when the Gaussian curvatures of the two metrics coincide [35, 46, 50–52]. Within these energetic considerations, there is a special group of elastic energy minimizers, called isometric immersions, that adopt exactly the Gaussian curvature of the reference metric, $a = \bar{g}$, such that their elastic energy scales as $t^3$ [53]. Nevertheless, isometric immersions do not always exist. In these cases, the energetic competition between the stretching and bending energies is more involved, and the total energy scales as $t^\alpha$ where $\alpha \leq 3$. The latter scenario was investigated in Ref. [20] by prescribing a discontinuous swelling profile, or equivalently a discontinuous reference metric, on the gel's surface. For this reference profile, isolated line elements on the gel attain multiple values and thus, isometric minimizers are prohibited.

Following Ref. [20], we consider a thin strip of an unswollen thickness $t$, width $w$ and length $2L$ that is subjected to a differential discontinuous swelling along the mid-line of the sample (see Fig. 1a). This discrete variation in the swelling profile is modeled by the following reference metric,

$$\bar{g}_{\alpha\beta} = h(z)^2(dy^2 + dz^2) \quad ; \quad h(z) = \begin{cases} \Phi_1 & 0 < z < L, \\ \Phi_2 & L < z < 2L, \end{cases} \tag{1}$$

where $(y, z) \in [-w/2, w/2] \times [0, 2L]$ are a set of Cartesian coordinates, and the constants $\Phi_1$ and $\Phi_2$ characterize the isotropic swelling of each region. In this formulation we assume that $\Phi_2 \geq \Phi_1$ such that a positive confinement parameter is defined by $\tau \equiv \Phi_2 - \Phi_1$. The system is stress free when $\tau = 0$.

This swelling profile induces non-uniform stretching and bending moduli on the gel's surface for the following two reasons. First, since the gel swells isotropically in all three dimensions (not just in 2D) the thicknesses from which the elastic deformations are measured are $\Phi_i t$ ($i = 1, 2$), and not just $t$. Second, the swelling of a gel changes the polymeric volume fraction, which in turn determines the elastic response of the sample [25, 54]; hence each strip has a different Young's modulus. In the following formulation, we define the spatially discontinuous stretching and bending moduli,

$$Y(z) = \begin{cases} Y_1, & 0 < z < L, \\ Y_2, & L < z < 2L, \end{cases} \quad ; \quad B(z) = \begin{cases} B_1, & 0 < z < L, \\ B_2, & L < z < 2L, \end{cases} \tag{2}$$

where $Y_i = E_i \Phi_i t/(1 - \nu^2)$ are the stretching moduli, $B_i = E_i(\Phi_i t)^3/[12(1 - \nu^2)]$ are the bending moduli, $E_i$ are the Young's moduli, and $\nu$ is the Poisson ratio. It is useful to define the ratio of the Young's moduli, $e \equiv E_2/E_1$, and the ratio of the swelling factors, $\phi \equiv \Phi_2/\Phi_1$, such that $Y_2/Y_1 = e\phi$ and $B_2/B_1 = e\phi^3$.
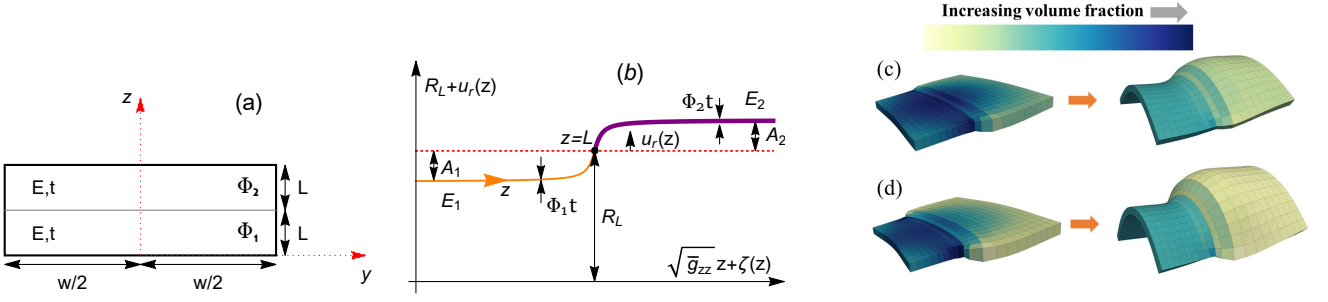
FIG. 1. Schematic overview of the system. (a) Top view of a flat system. A strip of unswollen thickness, $t$, width, $w$ and length, $2L$, is divided into two regimes at $z = L$ (gray line). At the initial, unswollen state, both strips have the same Young's modulus E. (b) Side view of a swollen 3D state. The orange (light thin) and purple (dark thick) curves correspond respectively to the strips with the low and high swelling constants, $\Phi_1$ and $\Phi_2$. The radius of the roll at $z = L$ is given by $R_L$. Deviations of the 3D shape from this radius are denoted by the radial displacement $u_r(z)$, where the coordinate $z \in [0, 2L]$ represents the arclength of the original, unswollen, state. In the limit of a small thickness, all the deformation is localized around the center point, $z = L$. Asymptotically, far away from the transition layer, the radial displacement, $u_r(z)$, approaches the constant amplitudes $A_1$ and $A_2$. Panels (c) and (d) reveal two results from our gLSM simulations [27] where one of the strips contains polymeric loops that unfold as the temperature is reduced and thereby, generate internal stresses in the gel. In the left plot of these figures, the internal stresses are too weak to cause buckling and therefore all the deformation remains in-plane. The right plots correspond to a lower temperature, where more loops are opened. This additional increase in excess-length increases the internal stresses in the gels and causes buckling. The final configurations are part of a body of revolution, whose cross-section is described in panel (b). The difference between panels (c) and (d) is in the numbers of the prescribed loops. The sample in panel (d) contains more loops (8 Kuhn segments) than in panel (c) (4 Kuhn segments), and hence, the final gradients at the center of (d) are steeper than the gradients in panel (c). Colors in these plots represent the polymeric volume fraction of the gel elements.

Although the initial flat state of the system does not encompass any axisymmetric properties, the experiments in Ref. [20] suggest that the final configuration is a body of revolution. These observations are also supported by our gLSM simulations, as shown in Figs. 1c and 1d. This final configuration consists of two cylindrical rolls that are connected by a transition layer around the discontinuous line of swelling, $z = L$. (We note that this body of revolution differs from the one considered in Ref. [55] in the sense that its axis of revolution does not intersect with a point on the body.)

Motivated by these experimental results, we assume that the 3D position vector to a point in the final configuration is given by,

$$\mathbf{f}(z, \theta) = [R_L + u_r(z)]\,\hat{\mathbf{r}} + [\sqrt{\bar{g}_{zz}}z + \zeta(z)]\hat{\mathbf{z}}, \qquad (3)$$

where $u_r$ is the out-of-plane displacement, $\zeta$ is the in-plane displacement, $R_L$ is the radius of the body at $z = L$ and $\hat{\mathbf{r}}$ is a unit vector in the radial direction (see Fig. 1b for a schematic illustration of these variables and parameters). While the final configuration, Eq. (3), is given in cylindrical coordinates, $(z, \theta)$, the reference metric, Eq. (1), is given in Cartesian coordinates, $(y, z)$. Thus, to complete the formulation we must transform the $y$-coordinate into the $\theta$-coordinate. To do this, we set $dy \to Rd\theta$ and define the regime of the azimuthal coordinate to be, $(z, \theta) \in [0, 2L] \times [-w/2R, w/2R]$, where $R$ is a constant reference radius. Under this transformation Eq. (1) reads,

$$\bar{g}_{\alpha\beta} = h(z)^2(dz^2 + R^2 d\theta^2) \quad ; \quad h(z) = \begin{cases} \Phi_1 & 0 < z < L, \\ \Phi_2 & L < z < 2L. \end{cases} \qquad (4)$$

Since for any constant value, $R$, the rest-length of a line element in the $\theta$-direction is equal to $\Phi_1 w$ (or $\Phi_2 w$), as was originally prescribed by Eq. (1) in the $y$-direction, $R$ is yet an unknown constant. In this analysis, it will be determined so as to minimize the total energy. By applying this transformation, we made an assumption that the rest configuration of the gel is always buckled in the azimuthal direction. Indeed, although this transformation preserves the reference Gaussian curvature, $K_{\bar{g}}$, it applies a constant bending moment on the azimuthal edges of the gel, i.e., the total elastic energy is not invariant under this transformation.

Using these definitions, the total energy of the system has two contributions. One is the work of internal forces to deform the lengths of in-plane line elements, and the second is the work of bending moments to deform the gel out of its initial flat position. This energy is given by [32, 55],

$$E = \frac{1}{2}\int_0^{2L}\int_{-w/2R}^{w/2R}[\sigma_{zz}\epsilon_{zz} + \sigma_{\theta\theta}\epsilon_{\theta\theta}]\sqrt{\bar{g}}d\theta dz + \frac{1}{2}\int_0^{2L}\int_{-w/2R}^{w/2R}[M_{zz}\phi_{zz} + M_{\theta\theta}\phi_{\theta\theta}]\sqrt{\bar{g}}d\theta dz, \qquad (5)$$

where the first and second terms correspond to the stretching and bending energies. In addition, $\sigma_{\alpha\beta}$ and $\epsilon_{\alpha\beta}$ are the in-plane stresses and strains, and $M_{\alpha\beta}$ and $\phi_{\alpha\beta}$ are the bending-moments and bending-strains ($\alpha, \beta = \theta, z$). The off-diagonal components of these tensors vanish by the assumed axisymmetry of the solution, Eq. (3), i.e., $\sigma_{z\theta} = M_{z\theta} = 0$ and $\epsilon_{z\theta} = \phi_{z\theta} = 0$.

In this linear elasticity formulation, the stresses and the bending moments are linearly related to the strains and the bending-strains by Hooke's law,

$$\sigma_{\alpha\beta} = Y[(1-\nu)\epsilon_{\alpha\beta} + \nu\epsilon_{\gamma\gamma}\delta_{\alpha\beta}], \tag{6a}$$
$$M_{\alpha\beta} = B[(1-\nu)\phi_{\alpha\beta} + \nu\phi_{\gamma\gamma}\delta_{\alpha\beta}], \tag{6b}$$

where $\delta_{\alpha\beta}$ is the Kronecker delta. To close the formulation, we need to relate the displacements $u_r$ and $\zeta$ to the strains. It was recently shown that the mathematical formulation of thin sheets that undergo axisymmetric deformations is considerably simplified if the 3D strain tensor is redefined [55]. Since the present problem falls under this axisymmetric category, we take advantage of this simplification and use Biot's strain [55–57] rather than the Green-St. Venant's strain [46, 47] to formulate the elastic energy. While the former strain tensor measures linear deviation of line elements from their rest values, the latter strain tensor measures the square of these deviations and therefore inherently includes quadratic terms in the displacement fields. We emphasize from the outset that although the choice of a strain tensor may have a qualitative effect on the structure of the elastic theory [55, 58], in the present problem, it does not alter the main conclusions. Nevertheless, Biot's strain is used here in order to simplify the presentation of some expressions, as is discuss further below. Biot's constitutive relations read,

$$\text{Nonlinear strains:} \quad \epsilon_{zz} = \frac{\sqrt{(\sqrt{\bar{g}_{zz}} + \partial_z\zeta)^2 + (\partial_z u_r)^2}}{\sqrt{\bar{g}_{zz}}} - 1, \tag{7a}$$

$$\epsilon_{\theta\theta} = \frac{R_L + u_r}{\sqrt{\bar{g}_{\theta\theta}}} - 1, \tag{7b}$$

$$\phi_{zz} = \frac{1}{\sqrt{\bar{g}_{zz}}}\frac{(\sqrt{\bar{g}_{zz}} + \partial_z\zeta)\partial_{zz}u_r - \partial_{zz}\zeta\partial_z u_r}{(\sqrt{\bar{g}_{zz}} + \partial_z\zeta)^2 + (\partial_z u_r)^2}, \tag{7c}$$

$$\phi_{\theta\theta} = \frac{1}{\sqrt{\bar{g}_{\theta\theta}}}\frac{\sqrt{\bar{g}_{zz}} + \partial_z\zeta}{\sqrt{(\sqrt{\bar{g}_{zz}} + \partial_z\zeta)^2 + (\partial_z u_r)^2}}, \tag{7d}$$

where the components of the reference metric are given by Eq. (4). Equations (7a) and (7b) measure the linear extension of a line element in the $z$ and $\theta$ directions. They are derived from the relation $\epsilon_{\alpha\alpha} = \sqrt{a_{\alpha\alpha}/\bar{g}_{\alpha\alpha}} - 1$, where $a_{\alpha\alpha} = \partial_\alpha\mathbf{f}\cdot\partial_\alpha\mathbf{f}$ is the metric of the final configuration and $\mathbf{f}$ is given by Eq. (3). Note that in these expressions and subsequent ones summation is not implied on repeated indices. Similarly, Eqs. (7c) and (7d) measure the change of the unit normal vector, $\hat{\mathbf{n}} = \frac{\partial_z\mathbf{f}\times\partial_\theta\mathbf{f}}{|\partial_z\mathbf{f}\times\partial_\theta\mathbf{f}|}$, along these two principal directions. They are defined by $\phi_{\alpha\alpha} = \sqrt{c_{\alpha\alpha}/\bar{g}_{\alpha\alpha}}$, where $c_{\alpha\alpha} = \partial_\alpha\hat{\mathbf{n}}\cdot\partial_\alpha\hat{\mathbf{n}}$ is the third fundamental form. (Different from Ref. [55], here, the displacements $u_r$ and $\zeta$ switch roles. $u_r$ is the out-of-plane displacement and $\zeta$ is the in-plane displacement.) Although the above formulation is derived in the framework of linear elasticity, i.e., under the assumption of small strains, the constitutive relations, Eqs. (7), are not linear. This is one of the consequences of the dimensional reduction process, from 3D to 2D, that on one hand lowers the dimensionality of the problem, but on the other hand adds non-linear terms that characterize the geometry of the final configuration.

If the gradients in the final configuration are changing sufficiently slowly, these non-linear constitutive relations can be simplified according to the FvK approximation, i.e., expansion of Eqs. (7) to leading order in the displacement gradients. In addition, since gels can swell significantly beyond their dry state, $\Phi_i = 1$, the amount of swelling, $\Phi_i - 1$, is in general of order one. Therefore, this FvK expansion is taken around the swollen state of an unconstrained gel and not around its dry state. In other words, each strip swells by a factor $\Phi_i$ up to small elastic deviations of order $\epsilon_{\alpha\beta}$. The reduced constitutive relations read,

$$\text{FvK strains:} \quad \epsilon_{zz} \simeq \frac{\partial_z\zeta}{\sqrt{\bar{g}_{zz}}} + \frac{(\partial_z u_r)^2}{2\bar{g}_{zz}}, \tag{8a}$$

$$\epsilon_{\theta\theta} = \frac{R_L + u_r}{\sqrt{\bar{g}_{\theta\theta}}} - 1, \tag{8b}$$

$$\phi_{zz} \simeq \frac{\partial_{zz}u_r}{\bar{g}_{zz}}, \tag{8c}$$

$$\phi_{\theta\theta} \simeq \frac{1}{\sqrt{\bar{g}_{\theta\theta}}}. \tag{8d}$$

We emphasize two points regarding this reduction. First, since $\epsilon_{\theta\theta}$ does not involve derivatives of the displacement fields, it remains unchanged compared to its nonlinear counterpart, Eq. (7b). Second, in the case where $u_r = 0$, the FvK strains, Eqs. (8), become equivalent to the nonlinear strains, Eqs. (7). The latter two properties result from using the Biot strain rather than the Green-St. Venant [55]. In fact, if one uses the latter strain tensor, the reduction of the nonlinear strains to Eqs. (8) requires additional assumptions, such as assumptions on the smallness of the displacements themselves and not just their gradients.

Lastly, different from solid materials, the Young's moduli of each strip depends strongly on the microscopic structure of the gel. For this reason gels of a homopolymer network are usually characterized by the initial (before swelling) number of cross-links, $c_o v_o$, and the initial and final (after swelling) polymeric volume fraction, $\phi_o$ and $\phi$ [25]. In the framework of linear elasticity, the latter two quantities are not independent because conservation of polymer mass implies that $\phi \simeq \phi_o \Phi_i^{-3}$; this relation becomes exact if one considers the isotropic expansion of an unconstrained gel. Substituting the latter relation into the shear modulus that is predicted from the linearized model of polymer gels [25] we find that

$$E_i \simeq 2(1 + \nu)(c_o v_o)_i \Phi_i^{-1}, \tag{9}$$

where we converted the shear modulus to a Young's modulus using $\mu_i = E_i/[2(1 + \nu)]$ [32]. Therefore, given the swelling $\Phi_i$ and the total number of cross-links, $(c_o v_o)_i$, within each strip, we can determine the Young's modulus.

In summary, the characteristic features of the system are specified by the geometric dimensions, $L$, $w$ and $t$, the swelling factors, $\Phi_1$ and $\Phi_2$, and the physical constants, $E_1$, $E_2$ and $\nu$. Given these parameters, the above formulation allows us, in principle, to minimize the elastic energy, Eq. (5), for a given set of constitutive equations, Eqs. (7) or (8), and the stress-strain relations, Eqs. (6). The minimization of the energy is carried out with respect to the two displacements, $u_r(z)$ and $\zeta(z)$, and the two constants $R_L$ and $R$. Once these unknowns are determined, the 3D configuration is given by Eq. (3).

In the next two sections, we use this formulation to obtain an approximate analytical solution to the 3D configuration of a buckled gel. We then compare these predictions to the results from our gLSM simulations and the experimental data of Ref. [20].

## III.   Approximate analytical solution in the FvK model

In this section we utilize the formulation of the previous section to derive an approximate solution to the problem. This solution is derived in the FvK approximation and is divided into two parts. In the first part, we solve the problem under the assumption that the gel is flat ($u_r = 0$). This solution is required in order to fix the value of $R_L$, which guarantees that when $\Phi_1 = \Phi_2$ ($\tau = 0$) the gel swells homogeneously in all three dimensions and the system becomes stress-free. In the second part, we relax this assumption ($u_r \neq 0$) and minimize the total energy, given $R_L$ from the first part. This minimization is taken under an assumed function for $u_r$ (variational ansatz), and yields the 3D configuration of the roll given the system's parameters.

### A.   Approximate solution to the flat state of a swollen bi-strip

Although the FvK strains and the nonlinear strains become identical when $u_r = 0$, the following analysis is only an approximate solution to the flat configuration and not an exact one. This is because we initially assumed that the final configuration is a body of revolution, Eq. (3). The limits of this approximation are discussed a posteriori at the end of this section.

Setting $u_r = 0$ in Eq. (3) reduces the final configuration into a cylinder with constant radius,

$$\mathbf{f}(z, \theta) = R_L \hat{\mathbf{r}} + [\sqrt{\bar{g}_{zz}} z + \zeta(z)]\hat{\mathbf{z}}, \tag{10}$$

where the in-plane displacement, $\zeta(z)$, and the constant $R_L$ are yet to be determined by minimization of the total energy. In order to calculate this energy we first reduce the constitutive relations, Eqs. (8), to their form in the flat state, and then substitute them into Eq. (5). This procedure gives

$$E = \frac{w}{2} \int_0^{2L} \left[ \sigma_{zz} \frac{\partial_z \zeta}{\sqrt{\bar{g}_{zz}}} + \sigma_{\theta\theta} \left( \frac{R_L}{\sqrt{\bar{g}_{\theta\theta}}} - 1 \right) \right] \bar{g}_{zz} dz + \frac{(B_1 + B_2)wL}{2R^2}, \tag{11}$$

where we have carried out the azimuthal integration in the stretching energy and the total integration in the bending energy.

Minimization of Eq. (11) with respect to $\zeta$ gives $\partial_z(\sqrt{\bar{g}_{zz}}\sigma_{zz}) = 0$. Since $\sigma_{zz}$ must vanish at the free boundaries, $z = 0$ and $z = 2L$, the latter equation can be integrated to give $\sigma_{zz} = 0$, on the entire gel. The solution to this zero stress equation is given by

$$\zeta(z) = \begin{cases} -\nu\,(R_L/R - \Phi_1)\,z + a/2, & 0 < z < L, \\ -\nu\,(R_L/R - \Phi_2)\,z - a/2, & L < z < 2L, \end{cases} \tag{12}$$

where the constant of integration, $a = (1+\nu)(\Phi_2 - \Phi_1)L$, is determined such that the $\hat{\mathbf{z}}$ component of $\mathbf{f}(z,\theta)$, Eq. (3), is continuous at $L$. Substituting Eq. (12) back into the energy, Eq. (11), and performing the remaining integration gives,

$$E = \frac{wL}{2}(1 - \nu^2)\left[Y_1\,(R_L/R - \Phi_1)^2 + Y_2\,(R_L/R - \Phi_2)^2\right] + \frac{(B_1 + B_2)wL}{2R^2}. \tag{13}$$

Equation (13) gives the complete dependence of the energy on the parameters, $R_L$ and $R$. Minimization of this energy with respect to $R_L$ gives the required result,

$$R_L = \frac{\Phi_1 + \phi e\Phi_2}{1 + \phi e}R. \tag{14}$$

Note that Eq. (14) is symmetric under the transformation of the two indices, i.e., $\Phi_1 \leftrightarrow \Phi_2$ ($\phi \leftrightarrow 1/\phi$) and $E_1 \leftrightarrow E_2$ ($e \leftrightarrow 1/e$). This is a consequence of the mirror symmetry in the problem around the axis $z = L$. This symmetry will be of further use in the next section when we choose the ansatz for the out-of-plane displacement, $u_r$.

Although we obtained our main result, Eq. (14), and can proceed to analyze the buckled state, we first characterize the flat state as it will provide us with information about the level of this approximation. Substituting $R_L$ back into the energy, Eq. (13), and normalizing by the system's parameters, we obtain the total energy of the flat configuration

$$\frac{2E}{E_1\Phi_1 twL} = \frac{\phi e}{1 + \phi e}(\Phi_2 - \Phi_1)^2 + \frac{(1 + \phi^3 e)(\Phi_1 t)^2}{12(1 - \nu^2)R^2}, \tag{15}$$

where the first and second terms on the right hand side of Eq. (15) correspond respectively to the stretching and bending energies. Since minimization of Eq. (15) with respect to $R$ gives a diverging radius, $R \to \infty$, the minimizing configuration corresponds to a state with finite stretching and zero bending, as expected from a flat sheet. In addition, substituting Eq. (14) into the in-plane displacement, Eq. (12), and then in the cylindrical configuration, Eq. (10), we obtain the 3D position vector of the gel. Up to a rigid translation, this vector reads,

$$\mathbf{f}(z,\theta) = \frac{(\Phi_1 + \phi e\Phi_2)}{1 + \phi e}R\hat{\mathbf{r}} + g(z)\hat{\mathbf{z}}, \quad ; \quad g(z) = \begin{cases} \left[\Phi_1 - \frac{\nu\phi e}{1 + \phi e}(\Phi_2 - \Phi_1)\right]z + a/2, & 0 < z < L, \\ \left[\Phi_2 + \frac{\nu}{1 + \phi e}(\Phi_2 - \Phi_1)\right]z - a/2, & L < z < 2L. \end{cases} \tag{16}$$

While the radial part of this 3D position vector diverges since $R \to \infty$, the component in the $\hat{\mathbf{z}}$-direction remains constant. In the case, when $\Phi_1 = \Phi_2 \equiv \Phi$, we have that $R_L = \Phi R$ and consequently $\epsilon_{zz} = \epsilon_{\theta\theta} = 0$, i.e., the gel swells isotropically in the two in-plane directions such that the width becomes $\Phi w$ and the total length $\Phi(2L)$. Keeping in mind that the thickness is also swollen by a factor $\Phi$, we obtain that an unconstrained gel is homogeneously swollen in all three dimensions.

Lastly, since $\sigma_{zz} = 0$ only the stress component in the azimuthal direction differs from zero. This stress is a constant in both strips and has a discontinuity at $z = L$,

$$\sigma_{\theta\theta}/(E_1\Phi_1 t) = \begin{cases} (\Phi_2 - \Phi_1)/[\Phi_1(1 + (\phi e)^{-1})], & 0 < z < L, \\ -(\Phi_2 - \Phi_1)/[\Phi_2(1 + (\phi e)^{-1})], & L < z < 2L. \end{cases} \tag{17}$$

This solution corresponds to two flat strips ($R \to \infty$) that are homogeneously stretched (or compressed) in the azimuthal direction. This distribution of stresses is similar to the resulting forces in a mechanical system that consist of two springs, connected in parallel, with different rest lengths and springs' constants. The analogy to a discrete system of linear springs (that holds even if one uses the nonlinear strains) is a consequence of using Biot's strain tensor, which measures linear deviations of line elements from their rest-lengths [55].

Equation (17) sheds light on our level of approximation in this flat-state solution, because in practice the azimuthal stress, $\sigma_{\theta\theta}$, must not be constant. This is due to two reasons. First, our solution violates the boundary condition of vanishing normal stress on the azimuthal edges of the gel, $\sigma_{\theta\theta}(z, \pm w/(2R)) = 0$. This violation arises because of the axisymmetric assumption, Eq. (10), that prohibits shear strains, and thereby, the dependence of the displacements

on the $\theta$-coordinates. Second, because the minimizing configuration acts to restore the prescribed rest length on each strip, and thereby to relax the in-plane stresses, we would expect $\sigma_{\theta\theta}$ to obtain a maximum value at $z = L$ and then decay to zero away from that maximum. Since in the flat state the solution does not depend on the gel's thickness, but only on the two in-plane dimensions, $w$ and $L$, we estimate that along the $L$-direction, the stress will decay to zero over a length that is comparable with $w$, see for example Ref. [59, p. 46]. In this case, our approximation, Eq. (14), holds as long as the strip's length is small compared to its width, $L \ll w$.

## B.  Approximate solution to a buckled state of a swollen bi-strip

Although the reference metric, Eq. (4), prescribes zero Gaussian curvature on each individual strip, the reference Gaussian curvature of the entire system, the bi-strip, is not zero. Instead, it has a sharp peak along the line of the discontinuity, $z = L$, where the gel is necessarily stretched [60]. Since the final configuration tends to adopt the Gaussian curvature of the reference metric, we anticipate each strip to be almost intrinsically flat, i.e., with zero Gaussian curvature, except at some transition region close to the line of discontinuity. These considerations, along with the experimental results, motivates the following variational ansatz for the radial displacement,

$$u_r(z) = \begin{cases} A_1\left[1 - (z/L)^{\alpha_1}\right], & 0 < z < L, \\ A_2\left[1 - (z/L)^{\alpha_2}\right], & L < z < 2L, \end{cases} \tag{18}$$

where $A_i$ and $\alpha_i$ $(i = 1, 2)$ are four variational constants, which are yet to be determined. The reason that the amplitude of $u_r$ is not symmetric around $z = L$ $(A_1 \neq A_2)$, is because of the different elastic moduli and swelling factors of the two strips.

We add two comments regarding the selection of this ansatz. First, in the limit of a small thickness we anticipate $u_r$ to be constant almost everywhere except at some transition layer close to the line of discontinuity. This behavior is manifested in Eq. (18) when $\alpha_i \gg 1$. In this case the polynomial terms can be approximated by decaying exponents, $(z/L)^{\pm\alpha_i} \simeq e^{\pm\frac{z-L}{\delta_i}}$, where $\delta_i$ are the lengths of the transition layers,

$$\delta_1 \equiv L/|\alpha_1| \quad ; \quad \delta_2 \equiv L/|\alpha_2|. \tag{19}$$

Indeed, in the following analysis we show that the variational constants scale as, $\alpha_i \propto t^{-4/5}$.

Second, although the radial displacement, Eq. (18), must be continuous at $L$, its derivatives can in general contain discontinuities. These discontinuities are dictated by the matching conditions between the two strips at $z = L$, which in our axisymmetric formulation require continuity of $\sigma_{zz}$ and $M_{zz}$ [61]. While the stress, $\sigma_{zz}$, depends on the first derivative of $u_r$, the bending moment, $M_{zz}$, depends on the second derivative of $u_r$. Thus, in general, $u_r$ has to be continuous up to its second derivative. However, in this analysis, we assume that the energetic cost to satisfy the continuity of the bending moments is a higher order correction. This assumption is motivated by recent studies that predicted the formation of boundary layers with negligible energetic cost [38, 55, 62, 63], and will further be verified by our numerical solution in the next section. Therefore, we demand that only the first derivative of $u_r$ is continuous at $z = L$. This condition $(A_1\alpha_1 = A_2\alpha_2)$ supplemented by the mirror symmetry of the system to an exchange of indices allows us to eliminate one of the unknown constants. For this reason we define

$$\alpha_1 = (A_2/R)\alpha \quad ; \quad \alpha_2 = (A_1/R)\alpha, \tag{20}$$

where the constant $\alpha$ is used to replace the two $\alpha_i$'s, and we divide the amplitudes, $A_i$ in Eq. (20) by the constant $R$ in order to obtain dimensionless numbers. We emphasize that this is just an approximate solution and at equilibrium the configuration must also satisfy continuity of the bending moment, $M_{zz}$, which involves second order derivatives.

To obtain the energy as a function of $A_i$, $R$ and $\alpha$, we first need to calculate the in-plane displacement, $\zeta$. To do this, we substitute the constitutive relations, Eqs. (8), into the energy, Eq. (5), and minimize it with respect to $\zeta$. Since $\zeta$ appears only in Eq. (8a), we obtain $\partial_z\sigma_{zz} = 0$, on each side of the bi-strip. This equation, along with the boundary conditions of vanishing stress at the gel's edges, $z = 0$ and $z = 2L$, imply that $\sigma_{zz} = 0$. This equation is solved separately in each strip, where the continuity condition of $\sigma_{zz}$ at $z = L$ is automatically satisfied. The solution reads,

$$\zeta(z) = \begin{cases} \frac{\nu(\Phi_1 - \Phi_2)}{1 + (\phi e)^{-1}}z - \frac{\nu A_1 z}{R} + \frac{A_1 L}{R}\left(\frac{\alpha_2\alpha A_2^2}{2\Phi_1(1 - 2\alpha_1)L^2}\left(\frac{z}{L}\right)^{\alpha_1 - 2} + \frac{\nu}{1 + \alpha_1}\right)\left(\frac{z}{L}\right)^{\alpha_1 + 1} + \frac{a}{2}, & 0 < z < L, \\ \frac{\nu(\Phi_2 - \Phi_1)}{1 + e\phi}z - \frac{\nu A_2 z}{R} + \frac{A_2 L}{R}\left(\frac{\alpha_1\alpha A_1^2}{2\Phi_2(1 - 2\alpha_2)L^2}\left(\frac{z}{L}\right)^{\alpha_2 - 2} + \frac{\nu}{1 + \alpha_2}\right)\left(\frac{z}{L}\right)^{\alpha_2 + 1} - \frac{a}{2}, & L < z < 2L, \end{cases} \tag{21a}$$

$$a = (1 + \nu)(\Phi_2 - \Phi_1)L + \frac{A_1^2 A_2^2 \alpha^2}{2LR^2}\left(\frac{1}{(1 - 2\alpha_2)\Phi_2} - \frac{1}{(1 - 2\alpha_1)\Phi_1}\right) + \frac{\nu\alpha_1\alpha_2 L(\alpha_2 - \alpha_1)}{(1 + \alpha_1)(1 + \alpha_2)\alpha}, \tag{21b}$$

where the constant of integration, $a$, Eq. (21b), is determined such that $\mathbf{f} \cdot \hat{\mathbf{z}}$ is continuous at $z = L$. When $u_r = 0$, this solution reduces to the flat state, Eq. (12), where $R_L$ is given by Eq. (14).

Second, we substitute the ansatz, Eq. (18), and the above solution, Eq. (21), back into the constitutive relations, Eqs. (8), and then into the energy expression, Eq. (5). This gives after integration, $2E/(E_1\Phi_1 twL) = E_s + E_b$, where

$$E_s = \left(\frac{A_1}{R} + \frac{\Phi_2 - \Phi_1}{1 + (\phi e)^{-1}}\right)^2 + \phi e\left(\frac{A_2}{R} - \frac{\Phi_2 - \Phi_1}{1 + \phi e}\right)^2$$
$$+ \frac{1}{2A_1 A_2 R\alpha}\left[3(\phi e A_2^3 - A_1^3) - \frac{4R(\Phi_2 - \Phi_1)}{1 + (\phi e)^{-1}}(A_1^2 + A_2^2)\right], \tag{22a}$$

$$E_b = \frac{(\Phi_1 t)^2}{12(1 - \nu^2)}\left(\frac{1 + \phi^3 e}{R^2} + \frac{A_1^2 A_2^2(A_2 - \phi e A_1)\alpha^3}{2L^4 R^3 \Phi_1^2}\right), \tag{22b}$$

are respectively the leading order corrections to the stretching and bending energies compared to the flat state, Eq. (15). Since we anticipate that $\alpha \gg 1$, Eqs. (22) and the following results are presented to leading order in powers of $1/\alpha$.

Third, we minimize the total energy, Eqs. (22), with respect to $A_i$, $R$ and $\alpha$. To leading order, the amplitudes $A_1$ and $A_2$ are obtained by minimization of the stretching energy, Eq. (22a), alone. This gives,

$$A_1 = -\frac{(\Phi_2 - \Phi_1)R}{1 + (e\phi)^{-1}}, \quad ; \quad A_2 = \frac{(\Phi_2 - \Phi_1)R}{1 + e\phi}. \tag{23}$$

When Eqs. (23) are substituted back into the stretching energy, Eq. (22a), we obtain two simplifications. (i) The first two terms in this energy cancel and its leading order becomes proportional to $1/\alpha$. (ii) Equation (22a) becomes independent of the reference radius, $R$. Thus, the total energy now depends on $R$ only through the bending term, Eq. (22b). Therefore, minimization of Eq. (22b) with respect to $R$ gives

$$R = 2^{1/4}\frac{(1 + \phi e)^{5/4}(1 + e\phi^3)^{1/4}\Phi_1^{1/2}(\Phi_2 - \Phi_1)^{-5/4}L}{e^{1/2}\phi^{1/2}(1 + e^2\phi^2)^{1/4}\alpha^{3/4}}. \tag{24}$$

Lastly, once Eqs. (23) and (24) are substituted back into Eqs. (22), we obtain the complete dependence of the energy on the parameter $\alpha$

$$\frac{2E}{E_1\Phi_1 twL} = \frac{(1 + \phi^2 e^2)(\Phi_2 - \Phi_1)}{2(1 + \phi e)\alpha} + \frac{\sqrt{2}\phi e(1 + e\phi^3)^{1/2}(1 + e^2\phi^2)^{1/2}\Phi_1 t^2(\Phi_2 - \Phi_1)^{5/2}\alpha^{3/2}}{12(1 - \nu^2)(1 + \phi e)^{5/2}L^2}. \tag{25}$$

Minimization of Eq. (25) with respect to $\alpha$ gives

$$\alpha = 2^{3/5}\frac{(1 + \phi e)^{3/5}(1 + \phi^2 e^2)^{1/5}}{\phi^{2/5}e^{2/5}(1 + e\phi^3)^{1/5}\Phi_1^{2/5}}(1 - \nu^2)^{2/5}(\Phi_2 - \Phi_1)^{-3/5}(L/t)^{4/5}. \tag{26}$$

Substituting Eq. (26) back into the reference radius, Eq. (24), and the energy, Eq. (25), we obtain the desired solution

$$R/L = 2^{-1/5}\frac{(1 + e\phi^3)^{2/5}(1 + e\phi)^{4/5}\Phi_1^{4/5}}{\phi^{1/5}e^{1/5}(1 + e^2\phi^2)^{2/5}}(1 - \nu^2)^{-3/10}(\Phi_2 - \Phi_1)^{-4/5}(t/L)^{3/5}, \tag{27a}$$

$$\frac{2E}{E_1\Phi_1 twL} = \frac{5}{6 \times 2^{3/5}}\frac{\phi^{2/5}e^{2/5}(1 + e\phi^3)^{1/5}(1 + e^2\phi^2)^{4/5}\Phi_1^{2/5}}{(1 + e\phi)^{8/5}}(1 - \nu^2)^{-2/5}(\Phi_2 - \Phi_1)^{8/5}(t/L)^{4/5}. \tag{27b}$$

As a self-consistency check, it can be verified that these expressions are invariants under an exchange of indices, as required by the mirror symmetry.

Equations (27) are the central results of this paper. They provide the explicit dependence of the radius, $R$, and the energy, $E$, on the various parameters of the system. We note that the scaling of $R$ and $E$ with $t$, $L$ and the confinement, $\tau = \Phi_2 - \Phi_1$, coincide with the prediction in Ref. [22] (see Sec. 3.5, case 2, in that paper), which analyzed a closely related system. Nevertheless, the above solution improves these results in two aspects: first, we have obtained the full expressions including prefactors and not just scaling laws, and second, we added the correction due to the different elastic moduli and thicknesses of the two strips, i.e., the dependence of the solution on the parameters $e$ and $\phi$.

This completes the analytical solution in the FvK approximation. In summary, given the geometrical parameters $t$ and $L$, the physical parameters $\nu$ and $e = E_1/E_2$, and the swellings, $\Phi_1$ and $\Phi_2$, the final configuration is given by Eq. (3), where the radius, $R_L$, and the reference radius, $R$, are given by Eqs. (14) and (27a). In addition, the displacements $u_r$ and $\zeta$ are given by Eqs. (18) and (21), respectively, where $A_i$ and $\alpha$, are calculated from Eqs. (23) and (26).
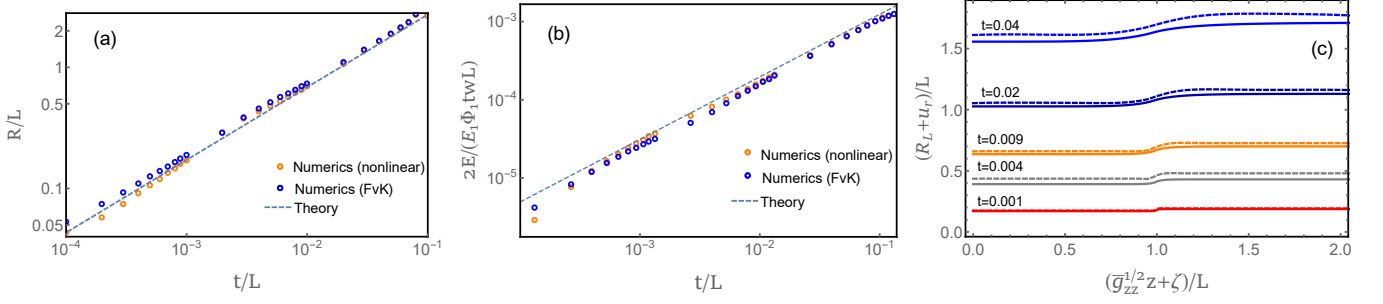
FIG. 2. Quantitative comparison between the analytical solution and the numerical optimization of the energy, Eq. (5). In all of these plots we use $\Phi_2 = 1.1$, $\Phi_1 = 1$, $\nu = 1/2$, $L = 1$, $\phi = \Phi_2/\Phi_1$ and , $e = \Phi_1/\Phi_2$ (we choose $(c_o v_o)_i = 1$ in Eq. (9)). (a) Log-Log plot of the normalized reference radius, $R/L$, as a function of the normalized thickness, $t/L$. The analytical prediction, Eq. (27a), is given by the dashed line and numerical results are indicated by orange (light) and blue (dark) circles, which correspond to nonlinear and FvK strains respectively. Both sets of strains give almost identical results, which agree nicely with the analytical solution. (b) Log-Log plot of the energy, Eq. (27b) dashed line, compared to the numerics. (c) The configuration of the sheet for several values of the thickness. The final configuration is a body of revolution that is obtained by rotation of these curves around the horizontal axis. The solid lines are the analytical predictions, Eq. (3), where the displacements are given by the FvK solution in Sec. III B. The dashed lines result from numerical optimization of the energy using the nonlinear strains, Eqs. (7).

## 1. Comparison with numerical simulations

Quantitative comparisons between the analytical predictions of the preceding section and the numerical optimization of the energy is presented in Figs. 2 (see Appendix A for further discussion on these numerical methods). The agreement between these numerical calculations and the above analytical solution validates our main assumption in this analysis, i.e., the variational ansatz, Eq. (18). In addition, it validates the following two assumptions that were utilized to simplify the final expressions. One is the continuity of $u_r$, that was assumed to be continuous only up to its first derivative, and second is the expansion in powers of $\alpha$. These quantitative predictions (and ones in the next section), sets the present analysis apart from previous studies, which focused on the qualitative behavior of the system. It is worth noting the important role played by the different elastic moduli, Eqs. (2), in the prefactors of our final solution, i.e., the dependence of Eqs. (27) on $e$ and $\phi$.

We also make quantitative comparisons between the theory and the gel lattice spring model (gLSM) simulations (see Fig. 3). The 3D gLSM combines a finite element approach and a finite difference approach and thus, allows us to numerically solve the elastodynamic equations that characterize the behavior of chemo-responsive polymer gels. The gLSM was recently augmented to simulate the behavior of LCST polymer networks that encompass thermo-responsive loops. The loops unfold as the temperature is decreased and thereby release the length that was stored within the folded configuration. The unfolding of the loops further increases the degree of local swelling and introduces new stresses into the system. Details about the simulations are given in Ref. [27]. In this study, all the simulations start from a flat and relaxed gel at $30^\circ[C]$, where the unswollen dimensions are $LxLx1$, i.e., the width and the length are equal, $w = L$, and the unswollen thickness is, $t = 1$. For this reason, lengths in the final configurations are measured in units of the unswollen thickness, $t$. This simulated sample is then divided into two strips, one that contains loops and one without loops, such that when the temperature is reduced the loop-containing strip swells more than the other side. The relation between the number of loops, the temperature, and the amount of swelling is given in Ref. [27]. Since the initial number of cross-links, $(c_o v_o)_i$ is identical in both strips, we use Eq. (9) to extract the Young's moduli ratio. This gives $e = \Phi_1/\Phi_2$ [64].

All plots present a systematic deviation of up to 10% between the theoretical line and the simulations. These discrepancies are attributed mainly to deviations from the Hookean model and to unavoidable shear stress at the transition region. Nonetheless, the quantitative agreement between the gLSM simulations and the analytical solution validates the assumptions that lead from the microscopic description of the gels, which account for the polymeric network structure and the internal forces within a single chain (the freely jointed chain model) [27], to the macroscopic description of thin elastic sheets, which coarse-grain these effects into a single elastic moduli.
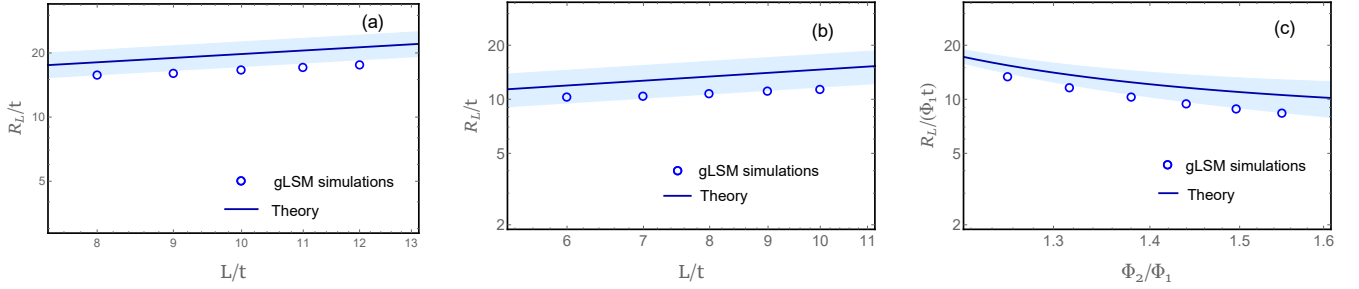
FIG. 3. Quantitative comparison between the approximated analytical solution (solid, blue line) and the gLSM simulations (blue circles). In all plots logarithmic scales are used for both axes. In panels (a) and (b) we plot the radius of the roll, $R_L/t$ (see Eq. (30)), as a function of its length $L/t$. The shaded (light blue) area around the theoretical radius $R_L/t$ corresponds to the minimum and maximum radii of a given shape, i.e., $(R_L + A_1)/t$ and $(R_L + A_2)/t$ where $A_i$ are given by Eqs. (23). In panel (a) one strip is embedded with four loops and the entire gel is cooled to $5^{\circ}[C]$ . Using Ref. [27] we convert this setup into our theoretical swelling factors, $\Phi_2 = 1.95$ and $\Phi_1 = 1.47$, where $\phi = \Phi_2/\Phi_1$ and $e = \Phi_1/\Phi_2$ (see Eq. (9)). The final configuration at $L = 10$ (third gLSM point) is plotted in Fig. 1c. In panel (b), we embed eight loops in one strip and cool the system to $15^{\circ}[C]$. Using Ref. [27], this gives $\Phi_2 = 2.14$ and $\Phi_1 = 1.38$, where $\phi$ and $e$ are as in panel (a). The 3D configuration in the case where $L = 10$ (first gLSM point from the right), is plotted in Fig. 1d. (c) The radius of the roll, $R_L/(\Phi_1 t)$, as a function of $\phi = \Phi_2/\Phi_1$. In this plot we keep the length constant, $L = 8$, and vary the number of loops within the gel from three to eight (left to right). While at three loops the temperature was lowered to $5^{\circ}[C]$ in order to obtain a buckled shaped, at the other points (four to eight loops) buckling into a roll are presented at $15^{\circ}[C]$.

## 2.  Limit to the validity of the FvK solution

We add one comment regarding the limits of our analytical analysis. The analytical solution in the FvK approximation breaks down when the thickness becomes sufficiently small (strong localization). This is because the deformation gradients are unbounded in this solution, i.e., the derivative of $u_r$ diverges as the thickness decreases, $\partial_z u_r \sim A_i \alpha \propto t^{-1/5}$. Consequently, the expansion in powers of small slopes, as in Eqs. (8), is unjustified below a critical thickness, $t_{\rm cr}$.

This critical thickness can be estimated from $\sigma_{zz}$ when the nonlinear strains are invoked. This is because to leading order, $\sigma_{zz}$ vanishes in both the nonlinear and the FvK models. Similar to Sec. III B where we showed that the FvK solution satisfies $\sigma_{zz} = 0$, we can minimize the stretching energy, the first term in Eq. (5), given the nonlinear strains, Eqs. (7)a and (7)b, and obtain the same equation. Substituting the nonlinear strains in this zero stress equation, $\epsilon_{zz} + \nu\epsilon_{\theta\theta} = 0$, gives

$$1 + \partial_z \zeta = \sqrt{\bar{g}_{zz}(1 - \nu\epsilon_{\theta\theta})^2 - (\partial_z u_r)^2} \simeq \sqrt{\bar{g}_{zz} - (\partial_z u_r)^2}, \tag{28}$$

where in the last equality, we used $\epsilon_{\theta\theta} \ll 1$ to simplify the term under the square root. Since the derivative of $u_r$ diverges, the right-hand side of Eq. (28) becomes imaginary at a critical thickness. This is the thickness at which we estimate that the FvK solution will deviate significantly from the nonlinear formulation. Using our analytical solution, we equate the right-hand-side of Eq. (28) to zero and solve for the critical thickness. This gives

$$t_{\rm cr}/L \simeq \frac{4e^2\phi^2(1 + e\phi^3)}{(1 + \phi^2 e^2)(1 + e\phi)^3\Phi_1^3}(1 - \nu^2)^{1/2}(\Phi_2 - \Phi_1)^3, \tag{29}$$

where we used $\bar{g}_{zz} = \Phi_1^2$ and $\partial_r u_r(L) = -A_1\alpha_1/L$. Using the mirror symmetry to exchange indices in Eq. (29), we can obtain the criterion from the second strip, however, it gives a lower bound for $t_{\rm cr}$.

Different from the FvK strains that allow the displacement gradients to grow indefinitely, we would expect the nonlinear formulation to saturate this non-regular behavior, because of the square root in Eq. (28). We note that this saturation was not depicted by our numerical simulations, Figs. 2, because in this case, $t_{cr}/L \simeq 4 \times 10^{-4}$, and the simulations almost reach their limit of validity. Indeed, when the thickness is reduced beyond this value, the localization in the elastic configuration almost becomes of order of the numerical lattice spacing.

## IV.  Comparison with experiments

In this section, we compare the analytical solution to the experimental data of Ref. [20]. In these experiments, the final configurations were characterized by their Gaussian curvature profile, $K(z)$, where $z$ is the axis of revolution.

Two direct measurements were taken with respect to this profile. One measurement is the radius of the roll when $K$ is equal to zero, $R_{\mathrm{K}=0}$. Second is a measurement of the transition region, $\Delta_{\mathrm{exp}}$ – the distance on the $z$-axis between the minimum and maximum values of $K$. Since our solution does not satisfy continuity of bending moments, i.e., the ansatz, Eq. (18), is discontinuous at its second derivative, we cannot extract a similar continuous profile as $K(z)$. Nevertheless, we conjecture that in the limit of a small thickness, the experimental measurements of $R_{\mathrm{K}=0}$ and $\Delta_{\mathrm{exp}}$ will coincide with our definition of $R_L$ and the transition layer, $\delta_1 + \delta_2$.

We summarize the main formulas for this comparison. First, the radius of the 3D shape at $z = L$, $R_L$, is given by Eq. (14),

$$R_L = 2^{-3/5} f(\phi, e, \Phi_1)(1 - \nu^2)^{-3/10}(\Phi_2 - \Phi_1)^{-4/5}(2L)^{2/5}t^{3/5}, \tag{30a}$$

$$f(\phi, e, \Phi_1) = \frac{(1 + e\phi^2)(1 + e\phi^3)^{2/5}\Phi_1^{9/5}}{\phi^{1/5}e^{1/5}(1 + e\phi)^{1/5}(1 + e^2\phi^2)^{2/5}}, \tag{30b}$$

where we used the reference radius $R$, from Eq. (27a), and we defined the function $f(\phi, e, \Phi_1)$ in Eq. (30b). It is straightforward to verify that this function complies with the mirror symmetry, $f(\phi, e, \Phi_1) = f(1/\phi, 1/e, \Phi_2)$. Second, in Eqs. (19), we defined two transition layers, one in each strip. Since these layers are given in the reference coordinates and the experimental transition region, $\Delta_{\mathrm{exp}}$, is measured in the deformed shape, we need to calculate the total lengths of these layers, $\delta_1 + \delta_2$, in the final configuration. To do this, we recall that the length of a line element along the $z$-direction is given by $\sqrt{a_{zz}}dz$, where $a_{zz} = \partial_z \mathbf{f} \cdot \partial_z \mathbf{f}$ is the $z$-component of the actual metric, i.e., the metric of the final configuration, Eq. (3). Therefore, the length of the transition layer in the final configuration is given by,

$$\Delta = \int_{L-\delta_1}^{L+\delta_2} \sqrt{a_{zz}}dz = \int_{L-\delta_1}^{L+\delta_2} \sqrt{\bar{g}_{zz}}(1 + \epsilon_{zz})dz \simeq \Phi_1\delta_1 + \Phi_2\delta_2, \tag{31}$$

where in the second equality we used the definition of the strain tensor, $\epsilon_{zz} = \sqrt{a_{zz}/\bar{g}_{zz}} - 1$, and in the third equality we used the fact that $\epsilon_{zz} \ll 1$ to estimate the integral. In addition, using Eqs. (19), (20), (23) and (26) we find that $\delta_1$ and $\delta_2$ are given by

$$\delta_1 = 2^{-3/5} f_1(\phi, e, \Phi_1)(1 - \nu^2)^{-2/5}(\Phi_2 - \Phi_1)^{-2/5}L^{1/5}t^{4/5}, \tag{32a}$$

$$\delta_2 = 2^{-3/5}\frac{f_1(\phi, e, \Phi_1)}{\phi e}(1 - \nu^2)^{-2/5}(\Phi_2 - \Phi_1)^{-2/5}L^{1/5}t^{4/5}, \tag{32b}$$

$$f_1(\phi, e, \Phi_1) = \frac{e^{2/5}\phi^{2/5}(1 + e\phi^3)^{1/5}\Phi_1^{2/5}}{(1 + e^2\phi^2)^{1/5}(1 + e\phi)^{-2/5}}. \tag{32c}$$

Keeping in mind that $t$ and $L$ are the independent parameters in the experiments, we find that Eqs. (30) and (32) depend on four unknown constants that must to be provided by the experimental setup, $\nu, \Phi_1, \Phi_2$ and $e$. These parameters are determined as follows. First, since gels are almost incompressible we choose $\nu = 1/2$ [65]. Second, the constants $\Phi_1$ and $\Phi_2$ are related to the experimental areal swelling ratios by $\Phi_1 = \Omega_{\mathrm{low}}^{1/2}$ and $\Phi_2 = \Omega_{\mathrm{high}}^{1/2}$. This is because areal swelling is defined as the ratio between the swollen ($\Phi_i^2 wL/2$) and the unswollen ($wL/2$) areas of an unconstrained gel [19]. The experimental values of these ratios are given by $\Omega_{\mathrm{low}} = 2.2$ and $\Omega_{\mathrm{high}} = 4.3$.

Third, we need to estimate the ratio of the Young's moduli, $e$. Although this value was not given explicitly in Ref. [20] (nor the number of cross-links), a later publication utilized elastocapillary bending of thin polymer films to extract their elastic coefficients [66]. These experiments used almost identical copolymer and solvent as in Ref. [20]. Given the volumetric swelling ratios $(\Phi_1)^3 \simeq 3.2$ and $(\Phi_2)^3 \simeq 8.9$, we find that $E_1 \simeq 800 kPa$ and $E_2 \simeq 300 kPa$ such that $e \simeq 0.37$ (see Table S3 in the supplemental material of Ref. [66]). Alternatively, following the same experiments, we could also obtain the number of cross-links from the extent of conversion, $p$. To do this, we convert the volumetric swelling into a UV dose [67] and then to $p$ (Table S3 and Fig. S2b in Ref. [66]). Considering Eq. (9), this gives a slightly different estimation, $e = (0.22/0.37)\Phi_1/\Phi_2 \simeq 0.42$, but yet within the range of the experimental error. Since the latter two values for $e$ change the roll's radii by negligible amount, we choose the former, direct, measurement in the following comparisons.

This completes the mapping of the various theoretical and experimental parameters. In summary we have,

$$\nu = 1/2, \qquad \Phi_1 = (2.2)^{1/2}, \qquad \Phi_2 = (4.3)^{1/2}, \qquad e \simeq 0.37, \qquad \phi = \Phi_2/\Phi_1. \tag{33}$$

Using these constants we can now verify that the experimental setup reconciles the main assumptions of our model. First, our model is derived in the context of linear elasticity, where Hookean stress-strain relations are invoked. Direct measurements of the gel's properties [16, 68] indicate that this assumption holds up to strains of $\pm 15\%$, beyond which neo-Hookean constitutive relations take place. Indeed, the strains in the experimental system only slightly deviate

from these limitations. From Eq. (7b) and the solution for $R_L$, Eq. (30), we obtain that the maximum azimuthal strain is

$$\epsilon_{\theta\theta}(L) = \begin{cases} (\Phi_2 - \Phi_1)/[(1 + (\phi e)^{-1})\Phi_1] \simeq 13\%, & \text{strip 1}, \\ -(\Phi_2 - \Phi_1)/[(1 + \phi e)\Phi_2] \simeq -19\%, & \text{strip 2}. \end{cases} \tag{34}$$

In addition, using $\sigma_{zz} = 0$ we obtain that $\epsilon_{zz}(L) = -\nu\epsilon_{\theta\theta}(L)$, and therefore the strain in the $z$-direction is always less than 10%. Second, we verify that the thickness does not cross its critical value, Eq. (29); below this value, nonlinear terms in the constitutive relations become important. Indeed, substituting the experimental constants, Eqs. (33), into Eq. (29) gives $t_{\mathrm{cr}}/L \simeq 2 \times 10^{-2}$, slightly below the experimentally used thicknesses.
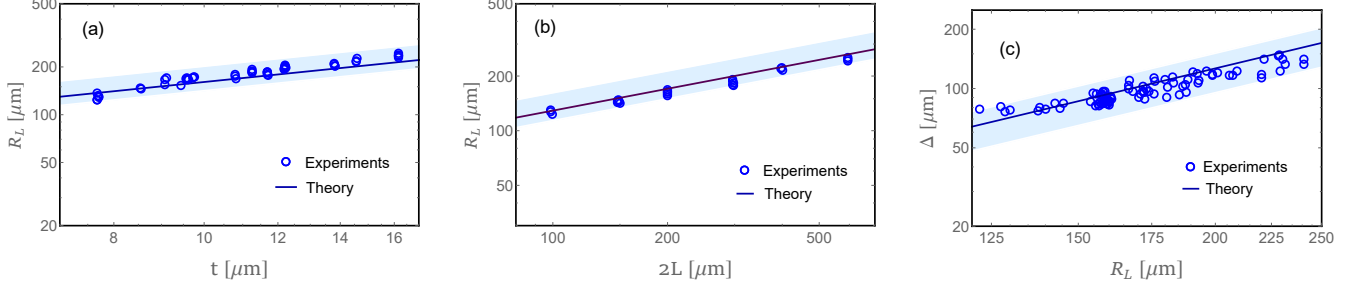


FIG. 4. Quantitative comparison between the approximated analytical solution and the experiments in Ref. [20]. In all panels the solid blue line is the analytical prediction and blue circles are points from the experimental data. The data in panels (a), (b) and (c) are taken respectively from Figs. 2C, 2D and 2B in Ref. [20]. In all plots logarithmic scales are used for both axes. We emphasize that the experimental radius $R_{\mathrm{K}=0}$ is defined slightly different than the analytical radius, $R_L$. For this reason we added a shaded area around the analytical prediction. This area is obtained when $R_L$ is replaced by either the minimum radius $R_L \to r_{\min} = \Phi_1 R$ or the maximum radius $R_L \to r_{\max} = \Phi_2 R$ of a given 3D shape, where $R$ is given by Eq. (27a). (a) The radius of the roll, Eq. (30a), as a function of the unswollen thickness, $t$, where $2L = 200\mu m$ is the total unswollen length of the gel. (b) The radius $R_L$, Eq. (30a), as a function of the unswollen total length, $2L$, where the unswollen thickness is $t = 11\mu m$. (c) The length of the transition layer, $\Delta$, as a function of the radius $R_L$. For a given thickness we calculate the parametric line $(R_L(t), \Delta(t))$, where $\Delta$ is given by Eqs. (31) and (32), and $R_L$ by Eqs. (30). The total length, $2L$, is the same as in panel (a).

Lastly, in Figs. 4, we plot the analytical predictions against the experimental data. Since the experimental radius $R_{\mathrm{K}=0}$ is not equivalent to $R_L$ we added a shaded area around the theoretical curve. This shaded area corresponds to the regime between the minimum and maximum radii of a predicted 3D shape, $r \in [r_{\min}, r_{\max}]$, where $r_{\min} = R_L + A_1$ and $r_{\max} = R_L + A_2$. While in Fig. 4a the radius $R_L$ is plotted as a function of the thickness, $t$, in Fig. 4b it is plotted as a function of the total length, $2L$. In the third plot, Fig. 4c, we compare the theoretical transition layer, Eqs. (31) and (32), and its experimental counterpart, $\Delta_{\mathrm{exp}}$. All plots present good agreement with our approximate solution. The scattering of the data around the predicted lines can be attributed to defects in the preparation of the gel's network such as the creation of loops, side-chains or heterogeneity in the length of the network size [69]. These defects can significantly change the elastic moduli of the gel.

## V.    Discussion

### A.    Classifications of the pattern and the elastic problem

Pattern formation on thin elastic sheets are universal in nature. For this reason much effort is devoted to classifying them into groups that share similar properties. Following Ref. [23], stress focusing structures on thin sheets are classified into two groups. One are vertices [70], which localizes the energy into isolated points, and second are ridges [71], which focus the energy along one-dimensional (1D) lines. Although the pattern we observe herein localizes the energy along a 1D line, $z = L$, and its total energy is equipartitioned between the stretching and bending components, as in a ridge, the other properties of the pattern do not coincide with the universal properties of ridges. This is due to the following three reasons. First, while in our solution the gradients of the displacement fields diverge as the thickness diminishes, in a ridge they remain finite. Therefore, the FvK solution of a ridge remains valid even in the asymptotic limit of vanishing thickness. Second, contrary to a ridge, the maximum strain in our system does not scale with the thickness size, i.e., Eq. (34) is independent on $t$. Third, while the total energy of our pattern scales as $t^{9/5}$ the energy that is accumulated in a ridge is much smaller and scales as $t^{8/3}$.

In addition to these 2D stress focusing patterns much attention was given to creases [72, 73], which are lines of discontinuity on the material that are endowed with a hinge-like behavior [74]. Different from ridges, which emerge spontaneously on a sheet with homogeneous elastic properties, creases are predesigned since they emanate from defects that are formed prior to the deformation. In general, creases are not necessarily accompanied by a transition layer that relaxes the stresses around them, and they do not necessarily involve the formation of a nonzero Gaussian curvature. Mathematically, while a ridge is associated with a continuous and differentiable surface (at least $\mathcal{C}^2$-surface), a crease creates an "origami-like" pattern, which has discontinuity in the first derivative ($\mathcal{C}^0$-surface).

The localized pattern observed herein retains properties of both groups, ridges and creases. On one hand, it has a ridge-like behavior since the energy is relaxed in a well defined transition layer around the line of discontinuity. On the other hand, similar to a crease, it emanates from a prescribed discontinuity in the swelling profile, Eq. (1), and consequently in the material's properties, Eqs. (2). Although this discontinuity manifests in-plane (the derivative of $\zeta$ and consequently the azimuthal stress are discontinuous at $L$), it only asymptotically emerges in the height function of the final configuration, i.e., the first derivative of $u_r$ diverges only in the limit of vanishing thickness. Although we asses that this creased-ridge pattern is more general in nature and can be found in other thin-sheet systems that are subjected to discontinuous swelling profiles, the characteristics of our solution (such as the scaling of the energy with the thickness) most probably depends on the setup of the system.

On top of the above classifications of stress focusing patterns, there are ongoing attempts to enumerate the elastic problems according to the strength and method by which the elastic sheet is confined [75, 76]. Given a system setup, the ultimate goal of this classification is to identify the set of morphologies that are theoretically accessible to it, apriori to any experiments or numerical simulations. A recent publication by Davidovitch et al. [77] suggests that the current problem falls under a class of "geometrically incompatible confinement" (GIC), which corresponds to non-developable deformations that emerge in the absence of external forces. This class is divided into two subgroups of weak and strong confinements depending on whether the confinement scales with the thickness size (weak) or not (strong). While in cases of strong confinement (and very small thickness), it is argued that the final configuration converges to an asymptotic isometry, i.e., a configuration in which the ratio between the stretching and bending energies diminishes as a power of the thickness, problems with a weak confinement presents more subtle stretching-bending interaction [42], such as equipartitioning of these energies. Given these suggestions, we asses that our system can be classified into a weak confinement GIC problem, at least where the thickness, $t/L$, is of order of the confinement, $\tau$. Indeed, this is roughly the regime where our gLSM simulations are performed and the main focus of the experimental data.

Nevertheless, in Sec. III B 2, we extended our weak GIC solution into the strong regime by fixing the confinement and reducing the gel's thickness. Since this naïve extension breaks down at $t \simeq t_{cr}$ we would expect this weak-to-strong transition to be accompanied by a morphological transition of the gel. This is because a roll that enters the nonlinear regime ($t \ll t_{cr}$) saturates the gradients of the displacements. In return, this saturation inhibits the creation of boundary layers around the line of discontinuity, and prevents efficient relaxation of the elastic energy. This inhibition can even lead to finite accumulation of stretching within the roll, in contrast to the expected behavior of a strong GIC solution. Although some attempts have been made to investigate morphological patterns on ultra-thin sheets close to lines of discontinuities [78], most of this area still remains unexplored. For this reason, further experiments and numerical investigations are required in order to reveal the accessible morphologies in this regime.

## B. Conclusions

Herein, we studied a 2D-to-3D morphological change in hydrogels that are subjected to discontinuous swelling profile. In particular, we followed the experimental setup of Ref. [20] and derived an analytical model that predicts the 3D configuration of a buckled gel. We demonstrated that such structures are well described by the elastic theory of thin and incompatible sheets when the theory contains the elastic moduli that account for the gel's polymeric structure. Our analytical results were verified by three independent comparisons, (i) comparison with the experimental data of Ref. [20], Figs. 4, (ii) numerical simulations that accounts for the complete elastodynamic behavior of gels (gLSM Ref. [27]), Figs. 3, and (iii) numerical optimization of the elastic energy, Figs. 2. All three comparisons present quantitatively good agreement with the analytical model. These quantitative predictions place the experimental setup of Ref. [20] as a benchmark in the analysis of pattern formation on thin gels since non-trivial 3D shapes are predicted analytically without any fitting parameters. Indeed, given our solution, this setup can be used to calibrate other experimental systems or to test the solutions of new finite-element methods. On a broader perspective, our analysis takes a step forward toward engineering the design of thin gels through use of analytical and numerical tools rather than experimental trial and error.

Several comments should be added regarding the analytical model. First, we summarize the main assumptions that allow the derivation of an analytically tractable theory. Initially, we applied the Kirchhoff-Love hypothesis to reduce the problem's dimensionality from 3D to 2D. The reduced theory not just allowed in-plane differential swelling of the

gel but also accounted for the spatially varying elastic moduli. We note that this spatial dependence of the stretching and bending moduli are essential components in achieving quantitative fits; considering a single moduli for the entire sheet significantly alters the theoretical predictions. Then, we focused on deformations that are along the principal axes of the stress (without shear strains), i.e., the final configuration is a body of revolution. Lastly, we reduced the constitutive relations between the strains and the displacement fields to their FvK approximation and assumed a variational ansatz for $u_r$.

Although our analysis is based on a particular ansatz, we were able to draw quantitative predictions on the final configuration. This is because regardless of the exact form of the localizing pattern, to leading order it can always be approximated by a polynomial expansion. We note that this expansion is properly introduced only if it is supplemented with the system's mirror symmetry to an exchange of indices and it correctly satisfies the boundary conditions. Furthermore, since our analysis is based on the FvK strains, Eqs. (8), and the nonlinearity in this model is manifested only by the quadratic term $(\partial_r u_r)^2$, assuming a variational ansatz for $u_r$, we essentially linearize the problem completely. Indeed, using this assumption, we obtained a linear equation for $\zeta$, which is exactly solvable. We note that this variational ansatz for the out-of-plane displacement was also used in Ref. [55] to derive a quantitative prediction for the boundary layer in an incompatible sheet with elliptic reference metric.

Moreover, in Eq. (22) we obtained that the energy of a buckled gel depends linearly on $A_i$ instead of the usual quadratic dependence on the out-of-plane displacement. This comes from the azimuthal strain, Eq. (8b), in which the out-of-plane displacement, $u_r$, appears linearly instead of quadratically. It emanates from the assumption that the final configuration is a body of revolution. Therefore, in our formulation, the flat state solution is always unstable against buckling in the radial direction. To explore the linear stability of the system, i.e., the flat-to-roll transition, this axisymmetric assumption must be relaxed. In addition, we note that although our analytical formulation is based on Biot's strain tensor, a similar system in Ref. [22] was analyzed using the Green-St. Venant's strain. Despite the differences between the two formulations, the dimensional analysis in the latter paper yields the same scaling laws as predicted herein. Therefore, we conclude that deviations between the two models, if any, are confined to an order which is beyond the small slope approximation. Whether beyond this FvK regime the deviations between the two models are significant is yet an open question [58, 79].

Lastly, this work can be extended in several directions and utilized to several applications, as we now discuss. First, an interesting aspect in the experiments of Ref. [20] revealed, in some samples, hysteresis of the 3D structure upon a temperature cycle, i.e., raising and lowering the temperature of a buckled-rolled gel in a cycle resulted in a metastable state. These interesting properties that result from thermal fluctuations of the system [80] are currently not part of our theoretical model and the gLSM simulations, and can be considered as a possible extension. Second, using a discrete swelling profile, the experimentalists in Ref. [20] were able to produce responsive micro-patterned hinges. Since these hinges are the building blocks of many technological applications, such as self-assembled robots [81] or origami patterns [82], it may be valuable to derive theoretical predictions to the relation between the swelling profile of a gel and the angles of the hinges. Third, since our analytical model predicts the numerical prefactors of the resulted 3D shape, and geometrical measurements of the final configuration are to some extent simpler than direct measurements of the elastic properties of the gel, our solution can be used to extract the mechanical properties of the gel, such as its Young's modulus or the Flory-Huggins interaction parameter. Fourth, as a fundamental pattern in thin sheets, it will be interesting to explore the formation of a ridge [71] on the boundary between two dissimilar materials.

### A. Numerical optimization of the total energy

The optimization of the energy, Eq. (5), follows the numerical model in Ref. [83], but includes two modifications. First, since only axisymmetric minimizers are anticipated we discretize a one dimensional (1D) segment of the elastic body instead of the entire 2D sheet, i.e., we consider a 1D line of length $2L$ that lies on the $z$ axis. Second, since we expect sharp gradients around the center point, $z \in [L - \epsilon, L + \epsilon]$ where $\epsilon \ll L$, whereas outside this regime the configuration is almost flat, the line is not discretized into equally spaced points. Instead, each strip is divided into $n = n_o + n_\epsilon$ points ($n - 1$ line elements) where $n_o$ and $n_\epsilon$ are the number of points outside and inside the localization region. For example, in the first strip we have $n_o$ points that are equally spaced in $z \in [0, L - \epsilon]$ and $n_\epsilon$ points that are equally spaced in $z \in [L - \epsilon, L]$.

The two displacements fields, $u_r(z)$ and $\zeta(z)$, and the components of the reference metric, $\bar{g}_{zz}$ and $\bar{g}_{\theta\theta}$, are then discretized on this 1D grid, such that the constitutive relations, Eqs. (7) or (8), and thereby the stress-strain relations, Eqs. (6), are converted into finite differences. Accordingly, the integration of the total energy, Eq. (5), becomes a discrete sum over all the line elements. Then, for given parameters, $\{\Phi_1, \Phi_2, \nu, \epsilon, L, n_o, n_\epsilon, e\}$, the energy is minimized with respect to $u_r$ and $\zeta$ ($2n$ discrete points for each field) and the constant reference radius, $R$, where we assume that $R_L$ is given by Eq. (14).

Starting from $t = t_{\max}$ and an initial guess that is given by the FvK solution, Sec. III, we look for the optimum minimizer using a Newton-based method that is incorporated inside the built-in function FindMinimum in *Mathematica*© [84]. At each successive iteration, we reduce the thickness by a given increment and use the preceding output of this function as an initial guess for the next iteration. This procedure is repeated until the gradients in the transition layer become too large compared with the numerical lattice spacing.

[1] A. Goriely, *The Mathematics and Mechanics of Biological Growth*, 1st ed. (Springer, 2017).
[2] J. Dervaux and M. Ben Amar, Phys. Rev. Lett. **101**, 068101 (2008).
[3] J. Dervaux, P. Ciarletta, and M. B. Amar, Journal of the Mechanics and Physics of Solids **57**, 458 (2009).
[4] A. J. Hughes, H. Miyazaki, M. C. Coyle, J. Zhang, M. T. Laurie, D. Chu, Z. Vavruov, R. A. Schneider, O. D. Klein, and Z. J. Gartner, Developmental Cell **44**, 165 (2018).
[5] M. Osterfield, X. Du, T. Schpbach, E. Wieschaus, and S. Y. Shvartsman, Developmental Cell **24**, 400 (2013).
[6] N. Murisic, V. Hakim, I. G. Kevrekidis, S. Y. Shvartsman, and B. Audoly, Biophysical Journal **109**, 154 (2015).
[7] H. Liang and L. Mahadevan, Proceedings of the National Academy of Sciences **108**, 5516 (2011).
[8] V. Mirabet, P. Das, A. Boudaoud, and O. Hamant, Annual Review of Plant Biology **62**, 365 (2011).
[9] M. Sahaf and E. Sharon, Journal of Experimental Botany **67**, 5509 (2016).
[10] S. Liu, Z. Yao, K. Chiou, S. I. Stupp, and M. Olvera de la Cruz, Proceedings of the National Academy of Sciences **113**, 7100 (2016).
[11] T. Savin, N. A. Kurpios, A. E. Shyer, P. Florescu, H. Liang, M. L., and C. J. Tabin, Nature **476**, 5762 (2011).
[12] L. Hufnagel, A. A. Teleman, H. Rouault, S. M. Cohen, and B. I. Shraiman, Proceedings of the National Academy of Sciences **104**, 3835 (2007).
[13] E. Hohlfeld and L. Mahadevan, Phys. Rev. Lett. **106**, 105702 (2011).
[14] E. K. Rodriguez, A. Hoger, and A. D. McCulloch, Journal of Biomechanics **27**, 455 (1994).
[15] L. Ionov, Materials Today **17**, 494 (2014).
[16] G. Puleo, F. Zulli, M. Piovanelli, M. Giordano, B. Mazzolai, L. Beccai, and L. Andreozzi, Reactive and Functional Polymers **73**, 1306 (2013).
[17] J. L. Drury and D. J. Mooney, Biomaterials **24**, 4337 (2003).
[18] J. R. Fuchs, B. A. Nasseri, and J. P. Vacanti, The Annals of Thoracic Surgery **72**, 577 (2001).
[19] J. Kim, J. A. Hanna, M. Byun, C. D. Santangelo, and R. C. Hayward, Science **335**, 1201 (2012).
[20] J. Kim, J. A. Hanna, R. C. Hayward, and C. D. Santangelo, Soft Matter **8**, 2375 (2012).
[21] Z. L. Wu, M. Moshe, J. Greener, H. Therien-Aubin, Z. Nie, E. Sharon, and E. Kumacheva, Nature Communications **4** (2013), 10.1038/ncomms2549.
[22] M. Moshe, E. Sharon, and R. Kupferman, Nonlinearity **26**, 3247 (2013).
[23] T. A. Witten, Rev. Mod. Phys. **79**, 643 (2007).
[24] V. V. Yashin and A. C. Balazs, Science **314**, 798 (2006).
[25] V. V. Yashin and A. C. Balazs, The Journal of Chemical Physics **126**, 124707 (2007).
[26] O. Kuksenok, V. V. Yashin, and A. C. Balazs, Phys. Rev. E **78**, 041406 (2008).
[27] S. Biswas, V. V. Yashin, and A. C. Balazs, Soft Matter **14**, 3361 (2018).
[28] M. Doi, Journal of the Physical Society of Japan **78**, 052001 (2009).
[29] R. Yoshida, Current Organic Chemistry **9**, 1617 (2005).
[30] P.-G. DeGennes, *Scaling Concepts in Polymer Physics* (Ithaca, N.Y.: Cornell University Press, 1979).
[31] S. Hirotsu, The Journal of Chemical Physics **94**, 3949 (1991).
[32] L. D. Landau and E. M. Lifshitz, *Theory of Elasticity 3rd Edition*, 3rd ed. (Butterworth-Heinemann, Oxford, 1986).
[33] A. L. Gol'Denveizer, *Theory of Elastic Thin Shells*, 1st ed. (Pergamon, 1961).
[34] D. P. Holmes, M. Roch, T. Sinha, and H. A. Stone, Soft Matter **7**, 5188 (2011).
[35] Y. Klein, E. Efrati, and E. Sharon, Science **315**, 1116 (2007).
[36] Y. Klein, S. Venkataramani, and E. Sharon, Phys. Rev. Lett. **106**, 118303 (2011).
[37] M. A. Dias, J. A. Hanna, and C. D. Santangelo, Phys. Rev. E **84**, 036603 (2011).
[38] J. Gemmer and S. C. Venkataramani, Soft Matter **9**, 8151 (2013).
[39] M. Pezzulla, S. A. Shillig, P. Nardinocchi, and D. P. Holmes, Soft Matter **11**, 5812 (2015).
[40] E. Cerda and L. Mahadevan, Phys. Rev. Lett. **90**, 074302 (2003).
[41] J. Huang, B. Davidovitch, C. D. Santangelo, T. P. Russell, and N. Menon, Phys. Rev. Lett. **105**, 038302 (2010).
[42] H. King, R. D. Schroll, B. Davidovitch, and N. Menon, Proceedings of the National Academy of Sciences **109**, 9716 (2012).

[43] B. Davidovitch, R. D. Schroll, D. Vella, M. Adda-Bedia, and E. A. Cerda, Proceedings of the National Academy of Sciences **108**, 18227 (2011).

[44] E. Sharon, B. Roman, M. Marder, G.-S. Shin, and H. L. Swinney, Nature **419**, 579 (2002).

[45] M. Marder, Foundations of Physics **33**, 1743 (2003).

[46] M. Marder, E. Sharon, S. Smith, and B. Roman, EPL (Europhysics Letters) **62**, 498 (2003).

[47] E. Efrati, E. Sharon, and R. Kupferman, J. Mech. Phys. Solids **57**, 762 (2009).

[48] P. G. Ciarlet, *An Introduction to Differential Geometry with Applications to Elasticity*, 1st ed. (Springer Netherlands, The address, 2005).

[49] M. M. Lipschutz, *Theory and problems of differential geometry (Schaum's outline series)*, 1st ed. (McGraw-Hill, The address, 1969).

[50] M. Pezzulla, G. P. Smith, P. Nardinocchi, and D. P. Holmes, Soft Matter **12**, 4435 (2016).

[51] M. Pezzulla, S. A. Shillig, P. Nardinocchi, and D. P. Holmes, Soft Matter **11**, 5812 (2015).

[52] S. Armon, H. Aharoni, M. Moshe, and E. Sharon, Soft Matter **10**, 2733 (2014).

[53] M. Lewicka, L. Mahadevan, and M. R. Pakzad, Proc. Roy. Soc. London A **467**, 402 (2010).

[54] M. E. Harmon, D. Kuckling, and C. W. Frank, Langmuir **19**, 10660 (2003).

[55] O. Oshri and H. Diamant, Phys. Rev. E **95**, 053003 (2017).

[56] O. Oshri and H. Diamant, Soft Matter **12**, 664 (2016).

[57] M. A. Biot, *Mechanics of incremental deformations*, 1st ed. (John Wiley & Sons, The address, 1965).

[58] J. A. Hanna, arXiv:1807.06426 (2018).

[59] S. Timoshenko and J. N. Goodier, *Theory of elasticity*, 2nd ed. (Mcgraw-Hill, 1951).

[60] One way to obtain the Gaussian curvature of a discontinuous metric is to choose $h(r)$ to be a continuous family of functions that asymptotically converge into a step function by tuning of some parameter. One example of such functions can be found in Ref. [22].

[61] More accurately, the boundary conditions are $\Phi_1 \sigma_{zz}^1 = \Phi_2 \sigma_{zz}^2$ and $\Phi_1 M_{zz}^1 = \Phi_2 M_{zz}^2$, where the superscripts 1 and 2 indicate that the stresses and the bending moments are calculated in different strips.

[62] J. A. Gemmer and S. C. Venkataramani, Nonlinearity **25**, 3553 (2012).

[63] E. Efrati, E. Sharon, and R. Kupferman, Phys. Rev. E **80**, 016602 (2009).

[64] In order to verify that the Eq. (9) holds in our simulation we also measured $E_1$ and $E_2$ (and therefore the ratio, $e$) directly from their force-displacement curves. While for small number of loops the value of $e$ agrees well with the predicted value of Eq. (9), at large number of loops we found deviation of up to 15%. These deviations are attributed to our numerical model, which uses freely jointed chain rather than the Gaussian model for polymer chains. Nevertheless, this deviation changes the theoretical prediction in Fig. 3 by negligible amount.

[65] I. I. Ward and J. Sweeney, *Mechanical Properties of Solid Polymers*, 2nd ed. (John Wiley & Sons, 2012).

[66] J. Bae, T. Ouchi, and R. C. Hayward, ACS Applied Materials & Interfaces **7**, 14734 (2015).

[67] We note that the UV dose as a function of the volumetric swelling ratio differs between Refs. [20] and [66]. This is due to a different light sources that were used for the cross-linking in the two experiments [85].

[68] M. A. Haq, Y. Su, and D. Wang, Materials Science and Engineering: C **70**, 842 (2017).

[69] D. Chan, Y. Ding, R. H. Dauskardt, and E. A. Appel, ACS Applied Materials & Interfaces **9**, 42217 (2017).

[70] E. Cerda and L. Mahadevan, Phys. Rev. Lett. **80**, 2358 (1998).

[71] A. E. Lobkovsky, Phys. Rev. E **53**, 3750 (1996).

[72] F. Lechenault, B. Thiria, and M. Adda-Bedia, Phys. Rev. Lett. **112**, 244301 (2014).

[73] M. A. Dias, L. H. Dudte, L. Mahadevan, and C. D. Santangelo, Phys. Rev. Lett. **109**, 114301 (2012).

[74] We note that the term 'crease' is used in the literature with multiple meanings, as for example the system in Ref. [86]. Here, a crease is used to describe an origami line defect.

[75] G. M. Grason and B. Davidovitch, Proceedings of the National Academy of Sciences **110**, 12893 (2013).

[76] E. Hohlfeld and B. Davidovitch, Phys. Rev. E **91**, 012407 (2015).

[77] B. Davidovitch, Y. Sun, and G. M. Grason, Proceedings of the National Academy of Sciences (2018), 10.1073/pnas.1815507116.

[78] O. Mahmood, B. Audoly, and S. Roux, Phys. Rev. Lett. **121**, 144301 (2018).

[79] H. G. Wood and J. A. Hanna, arXiv:1808.01310 (2018).

[80] D. Grossman, E. Sharon, and H. Diamant, Phys. Rev. Lett. **116**, 258105 (2016).

[81] S. Felton, M. Tolley, E. Demaine, D. Rus, and R. Wood, Science **345**, 644 (2014).

[82] J.-H. Na, A. A. Evans, J. Bae, M. C. Chiappelli, C. D. Santangelo, R. J. Lang, T. C. Hull, and R. C. Hayward, Advanced Materials **27**, 79 (2014).

[83] H. S. Seung and D. R. Nelson, Phys. Rev. A **38**, 1005 (1988).

[84] W. R. Inc., *Mathematica, Version 11.0*, champaign, IL, 2018.

[85] R. C. Hayward, private communication.

[86] P. Ciarletta, Nature Communications **9** (2018).